Computer & Robotics

A Fuzzy Fault-Tolerant Controller Design Based On Virtual Sensor for DC Microgrid

Alireza Galavizh [a], Amir Hossein Hassanabadi [a,*]

[a] *Faculty of Electrical, Biomedical and Mechatronics Engineering, Qazvin Branch, Islamic Azad University, Qazvin, Iran.*

Abstract

In This Paper, A Fault-Tolerant Control (FTC) Method Is Presented For A DC Microgrid With Constant Power Loads (Cpls) That Is Prone To Sensor Faults. This FTC Method's Main Idea Is Based On Hiding The Sensor Faults From The Controller Point Of View Using A Suitable Virtual Sensor. After Presenting The System's Nonlinear Model, The Model Is Then Converted To A Takagi-Sugeno (TS) Fuzzy Representation. The Nominal Controller Is Designed For The Fuzzy Model In The Form Of State Feedback, And The States Are Estimated Using A Suitable Observer. In The Event Of A Sensor Fault Detection, The Effects Of The Fault In The Control Loop Are Compensated By A Virtual Sensor. The Controller's Gains, The Virtual Sensor, And The Observer Are Designed Using Related Linear Matrix Inequalities (Lmis) And Applying Some Appropriate LMI Regions To Achieve Appropriate Performance. The Proposed Method Is An Active Fault-Tolerant Control (AFTC) Strategy In Which The Virtual Sensor Hides The Sensor Faults From The Controller And The Observer. In This Method, From The Controller's Point Of View, The Faulty System Plus The Virtual Sensor Acts As A Healthy System, And The Nominal Controller Continues To Its Work Without The Need To Be Reconfigured. The Efficiency Of The Proposed

Keywords*: Fault, Active fault-tolerant control, TS fuzzy, virtual sensor, DC microgrid.*

1.Introduction

The use of microgrids in various industries, such as shipbuilding and aircraft manufacturing, has made significant progress. The general definition of a microgrid can be expressed as a set of sources of energy production (wind turbine, solar panels, etc.), energy storage systems and loads, which is a controllable system that can be possible to be connected or disconnected from the grid [1-3]. Control of these systems is addressed in two modes: connected and islanded. In general, microgrids are divided into two categories: alternating current (AC) and direct current (DC).

Due to the existence of power transfer protocols, it is necessary to use an appropriate control strategy for microgrids' efficient performance. The control parameters in these systems are current, voltage, frequency and power [4, 5]. Many approaches have been proposed to control microgrids' voltage, frequency, and power, for example, PI-based controllers and H_2 / H_∞ robust controllers [6]. Design of suitable type of controllers in case of a

* Corresponding author Email: a.hassanabadi@qiau.ac.ir

fault or failure in the system is an important and challenging issue [7].

One of the most critical issues in the design of modern automatic control systems is the reliability of the system. All systems can be prone to faults due to unpredictable internal and external effects. In order to prevent the spread of these faults in the system, detecting the faults in the early stages is important. Early detection of a fault in the system can prevent the system from behaving more abnormally [8]. Due to the 10 for TS fuzzy model in [27]. Also, fault detection for fuzzy TS systems has been addressed[28-30]. Stabilizing problem for TS fuzzy system using the uniform uncertain sampling is addressed in [31].

The two main pillars of this article are: TS fuzzy modelling and fault-tolerant control. First, the nonlinear model of the microgrid is converted to a TS fuzzy model, and then by using an appropriate AFTC design based on a suitable virtual sensor, the fault in the system is compensated in an appropriate manner. To the best of authors' knowledge, AFTC for DC microgrids using a virtual sensor has not been designed yet. The reliable operation of the microgrid in the event of sensor faults and the ability of the control loop to maintain the stability and performance in the faulty condition is a vital requirement. Assuring the reliable operation of the system will be achieved by designing a suitable virtual sensor in this paper.

The remaining of the paper is organized as follows: In the second section, the modelling of the considered DC microgrid based on TS fuzzy model is presented. In the third section, controller, virtual sensor and observer design formulation for AFTC strategy is expressed. In the fourth section, the design of the controller, the virtual sensor and the observer based on LMI region is presented. In the fifth section, the efficiency of the proposed strategy is shown and sixth section concludes this paper.

2.System Modelling Based On Ts Fuzzy

DC microgrids is widely used in various industries including ships, electric aircrafts and the automotive industries. A microgrid consists of two basic parts: the load and the sources of energy production or storage (Figure 1).

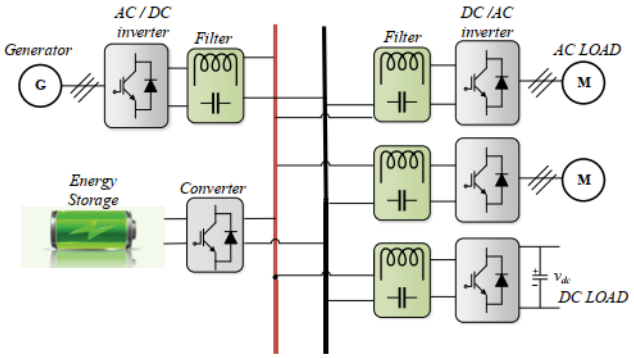

Fig. 1. General View Of The Microgrid [32]

The microgrid model considered in this paper is borrowed from [32] in which an electric model is used to model a microgrid which includes inductor, capacitor and electrical resistance (Figure 2). In Figure 2, the constant power loads (CPLs) section is connected to the energy storage system (ESS) by an RLC filter. Using KVL and KCL, the following equations can be written for CPL and ESS [32]:

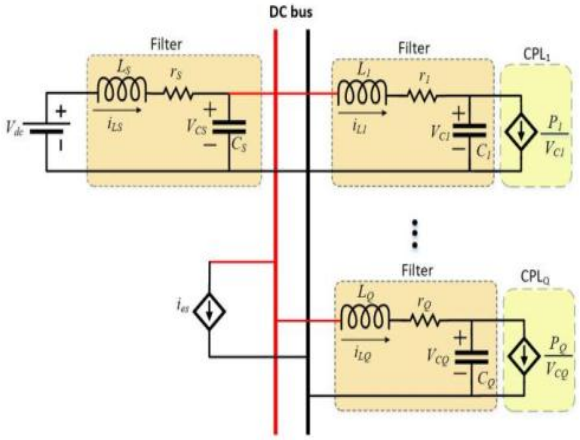

Fig. 2. Microgrid Modeling With Electrical Elements [18]

$$\begin{cases} \dfrac{di_{L,j}}{dt} = -\dfrac{r_j}{L_j} i_{L,j} - \dfrac{1}{L_j} v_{C,j} + \dfrac{1}{L_j} v_{dc} \\ \dfrac{dv_{c,j}}{dt} = \dfrac{1}{C_j} i_{L,j} - \dfrac{1}{C_j} \dfrac{P_j}{v_{C,j}} \end{cases} \quad (1)$$

$$\begin{cases} \dfrac{di_{L,s}}{dt} = -\dfrac{r_s}{L_s} i_{L,s} - \dfrac{1}{L_s} v_{C,s} + \dfrac{1}{L_s} v_{dc} \\ \dfrac{dv_{c,s}}{dt} = \dfrac{1}{C_s} i_{L,s} - \dfrac{1}{C_s} i_{e,s} \end{cases} \quad (2)$$

in which $i_{L,j}, v_{c,j}, i_{L,s}, v_{c,s}, V_{dc}, P_j$ and i_{es} are the load current, load voltage, source current, source voltage, constant voltage, constant power and

controller current in the load, respectively. By using the change of variables (3), equations (1) and (2) can be converted to (4) and (5).

$$\begin{aligned}\tilde{i}_{L,j} &= i_{L,j} - i_{L_0,j} \\ \tilde{v}_{C,j} &= v_{C,j} - v_{C_0,j} \\ \tilde{i}_{L,s} &= i_{L,s} - i_{L_0,s} \\ \tilde{v}_{C,s} &= v_{C,s} - v_{C_0,s}\end{aligned} \tag{3}$$

In (3), the equilibrium values are subtracted from the current and voltage values of the source and load. Thus:

$$\begin{cases} \dfrac{d\tilde{i}_{L,j}}{dt} = -\dfrac{r_j}{L_j}\tilde{i}_{L,j} - \dfrac{1}{L_j}\tilde{v}_{C,j} \\ \dfrac{d\tilde{v}_{C,j}}{dt} = \dfrac{1}{C_j}\tilde{i}_{L,j} + \dfrac{P_j}{C_j * v_{C_0,j}} \dfrac{\tilde{v}_{C,j}}{\tilde{v}_{C,j} - v_{C_0,j}} \end{cases} \tag{4}$$

$$\begin{cases} \dfrac{d\tilde{i}_{L,s}}{dt} = -\dfrac{r_s}{L_s}\tilde{i}_{L,s} - \dfrac{1}{L_s}v_{C,s} \\ \dfrac{d\tilde{v}_{c,s}}{dt} = \dfrac{1}{C_s}i_{L,s} - \dfrac{1}{C_s}\tilde{i}_{e,s} \end{cases} \tag{5}$$

Using (4) and (5), the state-space equations for CPL and ESS can be written as (6) and (7), respectively:

$$\frac{dx_j}{dt} = A_j x_j + d_j \bar{h}_j + A_{js} x_s \tag{6}$$

$$\frac{dx_s}{dt} = A_s x_s + b_s V_{dc} + b_{es} i_{es} + \sum_{j=1}^{Q} A_{cn} x_j \tag{7}$$

In (6) and (7), $x_j = \begin{bmatrix} i_{L,j} & v_{c,j} \end{bmatrix}^T$, $\bar{h}_j$, $x_s = \begin{bmatrix} i_{L,s} & v_{c,s} \end{bmatrix}^T$ and i_{es} are the load states, nonlinear terms, energy source states, and controller injection current, respectively and $\bar{h}_j$ is equal to $\dfrac{-1}{v_{c,j}}$. The general model of DC microgrid with the combination of (6) and (7) is written as (8) and (9):

$$\frac{d\tilde{X}_j}{dt} = \bar{A}\tilde{X} + \bar{D}h + \bar{B}_{es}\tilde{i}_{es} + \bar{B}_s \bar{V}_{dc} \tag{8}$$

$$\tilde{Y} = C\tilde{X} \tag{9}$$

Where $\tilde{X} = \begin{bmatrix} x_j & x_s \end{bmatrix}^T = \begin{bmatrix} i_{L,j} & v_{c,j} & i_{l,s} & v_{c,s} \end{bmatrix}^T$ is the system state vector and $u = i_{es}$ is the control signal and $\tilde{Y}$ is the output vector. The matrices A_{js} and A_{cn} are obtained from the statespace equations of the two load and source subsystems. The matrices of the model are:

$$\bar{A} = \begin{bmatrix} A_{j=1} & A_{(j=1)s} \\ A_{cn} & A_s \end{bmatrix} = \begin{bmatrix} \dfrac{-r_1}{L_1} & \dfrac{-1}{L_1} & 0 & \dfrac{1}{L_1} \\ \dfrac{1}{C_1} & 0 & 0 & 0 \\ 0 & 0 & \dfrac{-r_s}{L_s} & \dfrac{-1}{L_s} \\ \dfrac{-1}{C_s} & 0 & \dfrac{1}{C_s} & 0 \end{bmatrix} \tag{10}$$

$$\bar{B}_{es} = \begin{bmatrix} 0 \\ b_{es} \end{bmatrix} = \begin{bmatrix} 0 & 0 & 0 & \dfrac{-1}{C_s} \end{bmatrix}^T$$

$$\bar{D} = \begin{bmatrix} d_1 \\ 0 \end{bmatrix} = \begin{bmatrix} 0 & \dfrac{-P_1}{C_1} & 0 & 0 \end{bmatrix}^T$$

$$\bar{B}_s = \begin{bmatrix} 0 \\ b_s \end{bmatrix} = \begin{bmatrix} 0 \\ 0 \\ \dfrac{1}{L_s} \\ 0 \end{bmatrix}, \quad C = \begin{bmatrix} 0 & 1 & 0 & 0 \\ 0 & 0 & 0 & 1 \end{bmatrix}$$

There exists a combination of matrices A_j and A_s in $\bar{A}$ that were defined for load and source, respectively. The matrices $\bar{B}_{es}$, $\bar{B}_s$, $\bar{D}$ and C are also matrices that are written for general state-space equations and they are a combination of load and source variables. The state-space equations derived in (8)-(9) are nonlinear. There are many ways to control nonlinear systems. In this paper, due to the advantages of the multiple model approach, the proposed method is presented based on the TS fuzzy strategy [33]. TS fuzzy systems have recently become popular since they are an efficient tool for designing controllers for nonlinear systems. The most important feature of this strategy is the simplicity of fuzzy controller design and the possibility to convert conditions to LMI form [33]. If-then rules are

used to convert a state-space model to a TS fuzzy model. In this regard, the i[th] rule of the TS fuzzy model is shown as follows [34]:

$$\begin{aligned} &IF\ z_1(t)\ is\ M_{i1}\ \ and...and\ z_p(t)\ is M_{ip} \\ &Then\ \ \dot{\tilde{X}} = \tilde{A}_i\tilde{X} + \bar{D}h + B_{es}\tilde{i}_{es} + B_s\tilde{v}_{dc} \end{aligned} \quad (11)$$

Equations (8) and (9) are used to obtain TS fuzzy model for a DC microgrid with a single source and a constant power load. The following rule is used to calculate the number of TS fuzzy modes [32, 34]:

$$L = 2^Q \quad (12)$$

Since a CPL $(Q=1)$ is considered in the system, thus two TS models are defined $(L=2)$, which are weighted between 0 and 1 relating to the minimum and maximum of the parameter:

$$h_j = \frac{\tilde{v}_{c,j}}{v_{c_0,j}\left(\tilde{v}_{c,j} + v_{c_0,j}\right)} \quad (13)$$

In (13), $\tilde{v}_{c,j}$ is the capacitor voltage which is defined as the second parameter of vector $\tilde{X}$. To convert to the fuzzy TS model, the region $u_{\max}\tilde{v}_{c,1} \le h_1 \le u_{\max}\tilde{v}_{c,1}$ is considered which has its maximum and minimum bounds as:

$$u_{\min} = \frac{1}{v_{c_0,j}\left(\tilde{\omega}_{2,1} + v_{c_0,j}\right)} \quad (14)$$

$$u_{\max} = \frac{1}{v_{c_0,j}\left(-\tilde{v}_{c,1} + v_{c_0,j}\right)}$$

that $-\tilde{\omega}_{2,1} \le \tilde{v}_{c,1} \le \tilde{\omega}_{2,1}$ and h_1 is derived from (8), (9) and (14). In general, the sum of two parameters M_1 and M_2 is equal to one.

$$M_1 + M_2 = 1 \quad (15)$$

Thus:

$$\begin{cases} M_1 = \dfrac{u_{\max}\tilde{v}_{c,1} - h_1}{\left(u_{\max} - u_{\min}\right)\tilde{v}_{c,1}} \\ M_2 = \dfrac{h_1 - u_{\min}\tilde{v}_{c,1}}{\left(u_{\max} - u_{\min}\right)\tilde{v}_{c,1}} \end{cases} \quad (16)$$

So, the membership of the TS model is obtained regularly using two variables M_1 and M_2. In this case, in the rule (11), there are two clauses [34, 35]:

$$\begin{aligned} &if: \frac{h_1}{\tilde{v}_{c,1}}\ is\ \ u_{\min} \\ &Then: \dot{\tilde{X}} = \tilde{A}_1\tilde{X} + \bar{D}h + B_{es}\tilde{i}_{es} + B_s\tilde{v}_{dc} \\ &if: \frac{h_1}{\tilde{v}_{c,1}}\ is\ \ u_{\max} \\ &Then: \dot{\tilde{X}} = \tilde{A}_2\tilde{X} + \bar{D}h + B_{es}\tilde{i}_{es} + B_s\tilde{v}_{dc} \end{aligned} \quad (17)$$

The $\tilde{A}_1, \tilde{A}_2, B_{es}$ and B_s matrices are as follows:

$$\tilde{A}_1 = \begin{bmatrix} \frac{-r_1}{L_1} & \frac{-1}{L_1} & 0 & \frac{1}{L_1} \\ \frac{1}{C_1} & \frac{1}{C_1}u_{\min} & 0 & 0 \\ 0 & 0 & \frac{-r_s}{L_s} & \frac{-1}{L_s} \\ \frac{-1}{C_s} & 0 & \frac{1}{C_s} & 0 \end{bmatrix}, B_{es} = \begin{bmatrix} 0 \\ 0 \\ 0 \\ \frac{-1}{C_s} \end{bmatrix}$$

$$\tilde{A}_2 = \begin{bmatrix} \frac{-r_1}{L_1} & \frac{-1}{L_1} & 0 & \frac{1}{L_1} \\ \frac{1}{C_1} & \frac{1}{C_1}u_{\max} & 0 & 0 \\ 0 & 0 & \frac{-r_s}{L_s} & \frac{-1}{L_s} \\ \frac{-1}{C_s} & 0 & \frac{1}{C_s} & 0 \end{bmatrix} B_s = \begin{bmatrix} 0 \\ 0 \\ \frac{1}{L_s} \\ 0 \end{bmatrix} \quad (18)$$

Thus, the TS fuzzy model for a CPL which has two modes is obtained in the form of [32]:

$$\dot{\tilde{X}} = \sum_{i=1}^{r=2} M_i\left\{\tilde{A}_i\tilde{X} + \bar{D}h + B_{es}\tilde{i}_{es} + B_s\tilde{v}_{dc}\right\} \quad \textbf{(19)}$$

3. Aftc Design Based On The Virtual Sensor

An AFTC strategy is proposed to ensure that the system can tolerate a variety of faults, and its purpose is to maintain the stability and performance of the system. In AFTC, the controller has a better performance compared with PFTC, but it needs more computational power since the control loop is designed for nominal and faulty conditions separately. The TS fuzzy model of the considered

DC microgrid system consisting of both the CPL and the ESS [32] is as follows:

$$\dot{\tilde{X}} = \sum_{i=1}^{r=2} M_i \left\{ \tilde{A}_i \tilde{X} + \bar{D}h + B_{es}\tilde{i}_{es} + B_s \tilde{v}_{dc} \right\} \quad (20)$$

$$\tilde{Y} = C\tilde{X} \quad (21)$$

3.1. Faulty plant model

According to the types of faults, the tolerant control for the sensor faults in the system (20)-(21) is designed. Sensor faults affect the system output, which are modelled as a change in the matrix C:

$$\dot{\tilde{X}} = \sum_{i=1}^{r=2} M_i \left\{ \tilde{A}_i \tilde{X} + \bar{D}h + B_{es}\tilde{i}_{es} + B_s \tilde{v}_{dc} \right\} \quad (22)$$

$$\tilde{Y}_f = C_f \tilde{X} \quad (23)$$

3.2. TS fuzzy virtual sensor

Recently, the virtual sensor has been extended for nonlinear systems, which can be defined by the TS fuzzy system. The virtual sensor uses matrix P and vector y_Δ to reconstruct the faulty output signal as it is depicted in the block diagram of Figure 3.

The main idea of this FTC method is to reconfigure the faulty system so that the nominal controller sees the system as it is without fault and refuses to match the controller with the faulty plant. In general, the virtual sensor block makes it possible that the observer sees the same system as before when it became faulty [32, 33, 36].

The fuzzy virtual sensor is formulated as follows:

$$\dot{X}_v = \sum_{i=1}^{r=2} M_i \{ \tilde{A}_i X_v + \bar{D}h + B_{es}\tilde{i}_{es} + B_s \tilde{v}_{dc} + L_{v,i}\left(\tilde{Y}_f - Y_v\right) \} \quad (24)$$

$$Y_v = C_f X_v \quad (25)$$

in which X_v and Y_v are the state and output vector of the virtual sensor, respectively. The gain L_v is the virtual sensor gain matrix which will be designed later [33]. The proposed strategy is depicted in Figure 3.

If the following condition is met, the system output vector y_c can be reconstructed from $\tilde{Y}_f$ [33]:

$$rank\left(C_f\right) = rank\begin{pmatrix} C \\ C_f \end{pmatrix} \quad (26)$$

and y_c is reconstructed from $\tilde{Y}_f$ as follows [33]:

$$y_c = \sum_{i=1}^{r=2} M_i \left(P * \tilde{Y}_f + y_\Delta \right) \quad (27)$$

which $\tilde{Y}_f$ is the output of the faulty system. The matrix P is a design parameter that is calculated as follows:

$$P = CC_f^{\dagger} = CC_f^T \left(C_f C_f^T \right) \quad (28)$$

which $C_f^{\dagger}$ is the pseudo-inverse of the matrix C_f. The non-faulty matrix C can be reconstructed using the matrix P according to:

$$C = P * C_f \quad (29)$$

The signal y_Δ used in (27) can be obtained as follows [33]:

$$y_\Delta = C_\Delta X_v \quad (30)$$

Where

$$C_\Delta = C - P * C_f \quad (31)$$

When a sensor fault occurs, the virtual sensor reconstructs the output vector y_C from its input $\tilde{Y}_f$. A faulty system and a virtual sensor are called a reconfiguration scheme that are connected to the nominal controller [33].

3.3. TS fuzzy observer

The idea of the proposed FTC approach includes an observer to estimate the states of the nominal system. It is assumed that the system (20)-(21) is observable. The observer is formulated as follows [33, 37]:

$$\dot{\hat{X}} = \sum_{i=1}^{r=2} M_i \{ \tilde{A}_i \hat{X} + \bar{D}h + B_{es}\tilde{i}_{es} + B_s \tilde{v}_{dc} + L_{o,i}\left(y_c - \hat{Y}\right) \} \quad (32)$$

$$\hat{Y} = C\hat{X} \quad (33)$$

where $\hat{X}$ and $\hat{Y}$ are the state estimate and output estimate vectors respectively, which are estimated by the observer and $L_{o,i}$ are the observer gain matrices.

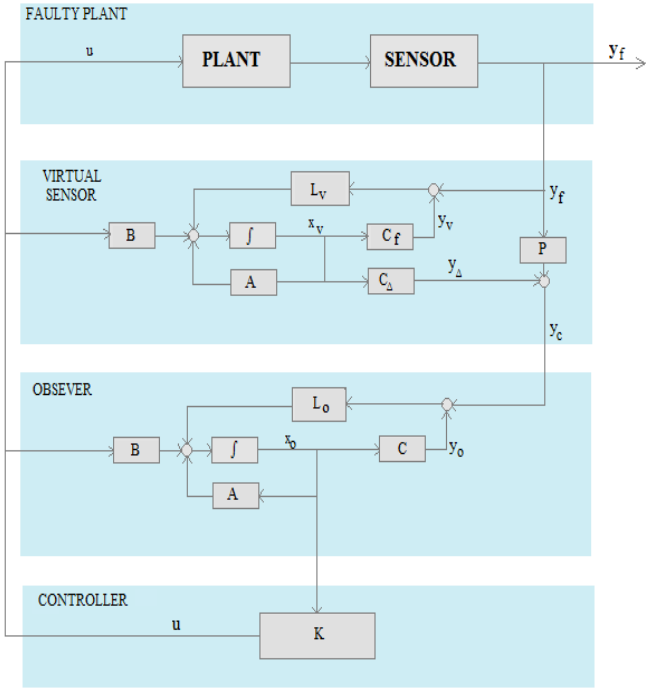

Fig. 3. FTC Strategy Using A Virtual Sensor

3.4. Fuzzy state feedback controller

The controller being used is a fuzzy state feedback one. It is assumed that the system (20) is controllable. The fuzzy state feedback controller is defined as:

$$u = \sum_{i=1}^{r=2} M_i \left(k_i * \hat{X} \right) \tag{34}$$

In this method, the vector $\hat{X}$, which is an estimate of the nominal system state, is used in both healthy and faulty modes [33].

4-Designing The Gains Using LMI Region

In this section, the D-stability condition is used to design the gains of the observer and the virtual sensor. One of the conditions for the stability of the system is that all the eigenvalues of the matrix $A \in \mathbb{R}^{n*n}$ be in the left side of the $j\omega$ axis. The LMI region is used to place the poles in the desired region intended by the designer. The LMI region has different forms regarding different regions [33, 38] such as conic sector, disk and circle. Here, the LMI region formed as a disk region with an appropriate radius and centre is used for designing the virtual sensor and the observer. The matrix $A \in \mathbb{R}^{n*n}$ is D-stable if there exists a matrix $X \in \mathbb{R}^{n*n}$ satisfying the following condition [38]:

$$\begin{bmatrix} -rX & qX + AX \\ qX + XA^T & -rX \end{bmatrix} < 0 \tag{35}$$

For a closed-loop dynamics described with a TS fuzzy model and the dynamic matrix M_i, condition (35) is reformulated as follows [38]:

$$\begin{bmatrix} -rX_i & qX_i + M_i X_i \\ qX_i + (M_i X_i)^T & -rX_i \end{bmatrix} < 0 \tag{36}$$

In (35) and (36), r and q are the radius and the origin of the disk, respectively which are shown in Figure 4. X_i for the virtual sensor and the observer are separately designed [38].
The following parameters for the controller, the virtual sensor and the observer are defined:

$$M_{1,i} = A_i - B_{es} k_i \tag{37-a}$$

$$M_{2,i} = A_i^T - C_{f,i}^T L_{v,i}^T \tag{37-b}$$

$$M_{3,i} = A_i^T - C_i^T L_{o,i}^T \tag{37-c}$$

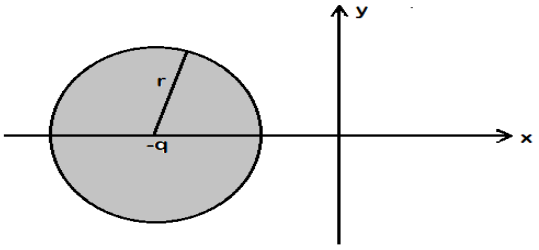

Fig. 4. Disk region $D_{(q,r)}$ [38]

By replacing each $M_{j,i}$ for $j = 2,3$ separately in the LMIs (36) and (37), the related constraints can be derived designing the virtual sensor and the observer. By doing so, some bilinear matrix inequalities (BMIs) are obtained due to the existence of multiplication of some variables. This difficulty is tackled by some change of variables.
The gains of the virtual sensor are obtained using the LMI presented in (36) for $M_{2,i}$:

$$\begin{bmatrix} -rX_{2,i} & qX_{2,i} + M_{2,i} X_{2,i} \\ qX_{2,i} + (M_{2,i} X_{2,i})^T & -rX_{2,i} \end{bmatrix} < 0 \tag{38}$$

By replacing (37-b) in (38):

$$\begin{bmatrix} -rX_{2,i} & -qX_{2,i} + (A_i^T - C_f^T L_{v,i}^T) X_{2,i} \\ qX_{2,i} + ((A_i^T - C_f^T L_{v,i}^T) X_{2,i})^T & -rX_{2,i} \end{bmatrix} < 0 \tag{39}$$

and defining the new variables:

$$W_{2,i} = L_{v(1,i)}^{T} X_{2,i} \tag{40}$$

the following LMIs is obtained:

$$\begin{bmatrix} -rX_{2,i} & qX_{2,i} + (A_i^T X_{2,i} - C_f^T W_{2,i}) \\ qX_{2,i} + (A_i^T X_{2,i} - C_f^T W_{2,i})^T & -rX_{2,i} \end{bmatrix} < 0 \tag{41}$$

After solving these LMIs, the virtual sensor gains are calculated as follows:

$$L_{v(1,i)} = \left[W_{2,i} X_{2,i}^{-1} \right]^T \tag{42}$$

The observer gains are calculated with the following formulation:

$$\begin{bmatrix} -rX_{3,i} & qX_{3,i} + M_{3,i} X_{3,i} \\ qX_{3,i} + (M_{3,i} X_{3,i})^T & -rX_{3,i} \end{bmatrix} < 0 \tag{43}$$

By substituting (37-c) in (43):

$$\begin{bmatrix} -rX_{3,i} & -qX_{3,i} + (A_i^T - C_i^T L_{o,i}^T) X_{3,i} \\ qX_{3,i} + ((A_i^T - C_i^T L_{o,i}^T) X_{3,i})^T & -rX_{3,i} \end{bmatrix} < 0 \tag{44}$$

and defining the new variables:

$$W_{3,i} = L_{o(1,i)}^{T} X_{3,i} \tag{45}$$

the following LMIs are resulted:

$$\begin{bmatrix} -rX_{3,i} & qX_{3,i} + (A_i^T X_{3,i} - C_i^T W_{3,i}) \\ qX_{3,i} + (A_i^T X_{3,i} - C_i^T W_{3,i})^T & -rX_{3,i} \end{bmatrix} < 0 \tag{46}$$

After solving these LMIs, the observer gains are obtained as follows:

$$L_{o(1,i)} = \left[W_{3,i} X_{3,i}^{-1} \right]^T \tag{47}$$

State feedback controller is designed with the following LMI region [32] which places the closed loop poles in the region depicted in Figure 5:

$$T \otimes P_{1,i} + G \otimes (P_{1,i} M_{1,i}) + G^T \otimes (P_{1,i} M_{1,i})^T < 0 \tag{48}$$

where:

$$T = \begin{bmatrix} 2\lambda & 0 & 0 & 0 \\ 0 & 2\lambda & 0 & 0 \\ 0 & 0 & 0 & 0 \\ 0 & 0 & 0 & 0 \end{bmatrix}, \quad G = \begin{bmatrix} 1 & 0 & 0 & 0 \\ 0 & 1 & 0 & 0 \\ 0 & 0 & \sin(\theta) & \cos(\theta) \\ 0 & 0 & -\cos(\theta) & \sin(\theta) \end{bmatrix}$$

and λ and θ are shown in Figure 5.

By substituting (37-a) in (48):

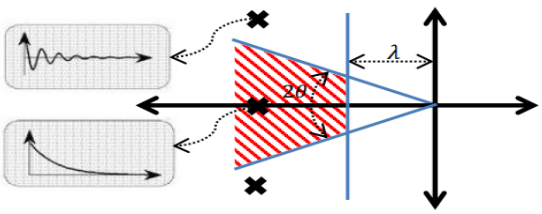

Fig. 5. Proposed region for placing the closed loop poles [32]

$$T \otimes P_{1,i} + G \otimes (P_{1,i}(A_i - B_{es} k_i)) + G^T \otimes (P_{1,i}(A_i - B_{es} k_i))^T < 0 \tag{49}$$

and defining the new variables:

$$X_{1,i} = P_{1,i}^{-1} \tag{50}$$

$$W_{1,i} = k_i X_{1,i} \tag{51}$$

(49) is converted to:

$$\begin{aligned} & T \otimes X_{1,i} + G \otimes (A_i X_{1,i}) \\ & - G \otimes (B_{es} W_{1,i}) \\ & + G^T \otimes (X_{1,i} * A_i^T) \\ & - G^T \otimes (W_{1,i}{}^T * B_{es}{}^T) < 0 \end{aligned} \tag{52}$$

After solving LMIs (52), the controller gains are obtained as:

$$k_{1,i} = W_{1,i} X_{1,i}^{-1} \tag{53}$$

The designed fault tolerant control system including the fuzzy state feedback controller, the fuzzy observer and the fuzzy virtual sensor actively tolerates the sensor faults. This is accomplished by hiding the faults from the observer and the controller by means of the virtual sensor.

4. Simulation

The microgrid used as a case study in this paper is borrowed from [11] with the same numerical values. The numerical values of the matrices $\tilde{A}_1$, $\tilde{A}_2$, B_{es} and B_s are equal to:

$$\tilde{A}_1 = \begin{bmatrix} -27.848 & -25.316 & 0 & 25.316 \\ 2000 & 2.0859 & 0 & 0 \\ 0 & 0 & -27.848 & -25.316 \\ -2000 & 0 & 2000 & 0 \end{bmatrix}$$

$$\tilde{A}_2 = \begin{bmatrix} -27.848 & -25.316 & 0 & 25.316 \\ 2000 & 2.6935 & 0 & 0 \\ 0 & 0 & -27.848 & -25.316 \\ -2000 & 0 & 2000 & 0 \end{bmatrix} \tag{54}$$

$$B_{es} = \begin{bmatrix} 0 \\ 0 \\ 0 \\ -2000 \end{bmatrix}, \quad B_s = \begin{bmatrix} 0 & 0 & 25.316 & 0 \end{bmatrix}^T$$

These matrices are derived from (10). The numerical values of the obtained controller, virtual sensor and observer gains are given in

Table 1. These gains are designed using the related LMI regions. The area which has been selected for placing the controller poles is as shown in Figure 5 with the following parameters:

$\lambda = 8$ and $\theta = \pi / 3$

The selected region for placing the virtual sensor poles is a circle with:

$r_{vietual\,sensor} = 70$ and $q_{vietual\,sensor} = 50$

and the selected region for placing the observer poles is a circle with:

$r_{observer} = 40$ and $q_{observer} = 30$

The selected regions have the best efficiency and it should be noted that the **SEDUMI** solver[39] has been used for solving the LMIs in YALMIP toolbox [40].

The main scenario of the simulation consists of two parts: a) non-faulty system b) faulty system. The total simulation time is 2 seconds. This operation time includes: nominal system stabilization, fault diagnosis and fault tolerant control with virtual sensor which is activated when the fault is detected. The values of the two weighting parameters M1 and M2 are shown in Figure 6.

Table 1
Gain table

Parameters	Gain
k_1	$\begin{bmatrix} -3.5394 & 0.47724 & -0.97676 & -0.61639 \end{bmatrix}$
k_2	$\begin{bmatrix} -3.5103 & 0.47792 & -0.97901 & -0.61425 \end{bmatrix}$
$L_{o,1}$	$\begin{bmatrix} -25.314 & 25.316 \\ 32.15 & -0.0010185 \\ 0.0023116 & -25.314 \\ -0.0010521 & 32.151 \end{bmatrix}$
$L_{o,2}$	$\begin{bmatrix} -25.314 & 25.316 \\ 32.15 & -0.0010231 \\ 0.0023117 & -25.314 \\ -0.0010413 & 32.151 \end{bmatrix}$
$L_{v,1}$	$\begin{bmatrix} -50.144 & 50.632 \\ 144.11 & -0.10041 \\ 0.4875 & -50.144 \\ -0.10039 & 144.21 \end{bmatrix}$
$L_{v,2}$	$\begin{bmatrix} -50.144 & 50.632 \\ 144.11 & -0.1004 \\ 0.4875 & -50.144 \\ -0.10039 & 144.21 \end{bmatrix}$

The type of fault that is considered in this scenario is a multiplicative sensor fault that occurs in 0.6 seconds and effects the output as follows:

$$\tilde{Y}(t) = \begin{cases} C\tilde{X} & for \quad t < 0.6_{\text{sec}} \\ C_f \tilde{X} & for \quad t \geq 0.6_{\text{sec}} \end{cases} \tag{55}$$

where $C_f = 0.5C$. The main steps of the simulation are as follows: First, the non-faulty system is stabilized and until the occurrence of the sensor fault only the observer is active with the nominal plant. In this case, the observer estimates the non-faulty outputs as depicted in Figure 7.

The virtual sensor is inactive until the detection of the sensor faults according to evaluating the residual signal. The residual signal, is calculated as follows:

$$r = W\left(\tilde{Y}_f(t) - \hat{Y}(t)\right) \tag{56}$$

where W is a weight matrix to shape the residual. A few moments after 0.6 seconds, the sensor fault is detected based on the residual signal, as it is shown in Figure 8.

As can be seen in Figure 8, the residual is zero until the time of 0.6 second which shows that there is no fault until this time. But after 0.6 second, due to the occurrence of the faults in both sensors, the residual responds to the faults and become nonzero. After detecting the sensor faults according to the residual, the task of the virtual sensor is to hide the faults from the controller and the observer.

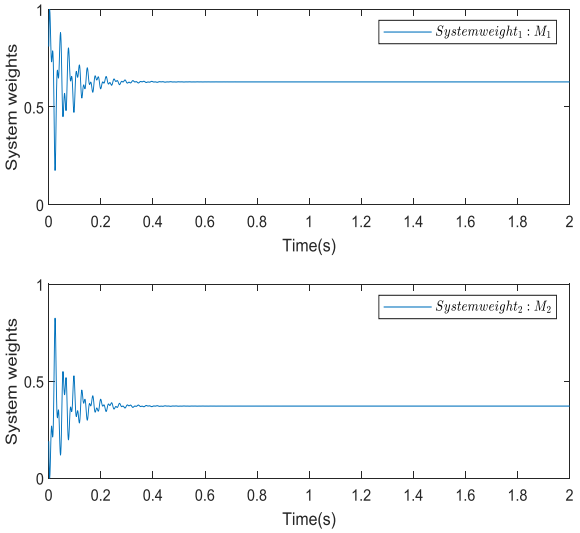

Fig. 6. Parameters M_1 and M_2

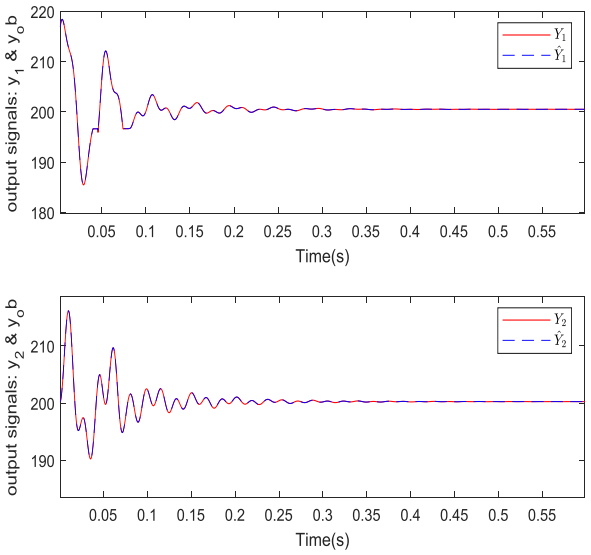

Fig. 7. Output of the nominal plant and observer in the absence of faults

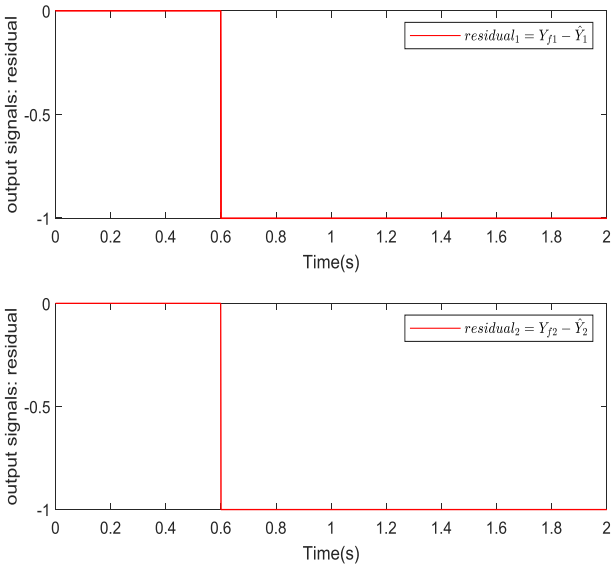

Fig. 8. Residual signal

The outputs of the virtual sensor after detecting the sensor faults is depicted in Figure 9. The activation of the virtual sensor happens after a change in the residual value from zero which is related to a situation of detecting a fault in the system. Therefore, according to Figure 9, the task of the virtual sensor is to provide the actual output values without fault after detection of sensor faults in the system.

The outputs of the healthy/faulty plant, the virtual sensor and the observer are depicted in Figure 10 which fully demonstrates the successfulness of the FTC strategy based on the designed fuzzy virtual sensor. As it is seen in Figure 10, the virtual sensor is inactive for up to 0.6 seconds and the estimated output has converged to real outputs. After 0.6 seconds onwards, the output has become faulty and the virtual sensor is activated.

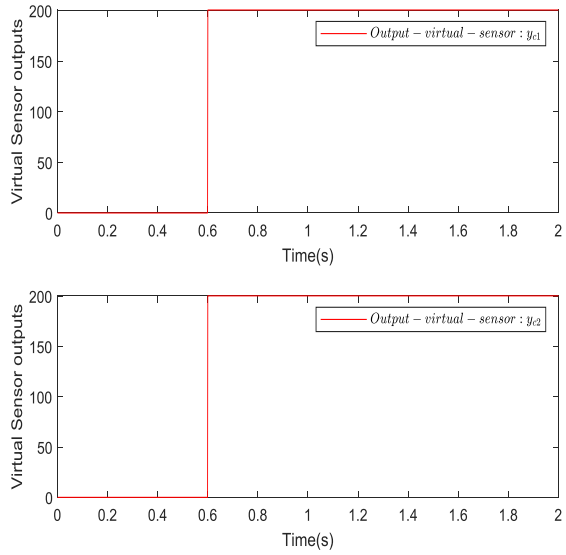

Fig. 9. Virtual sensor outputs

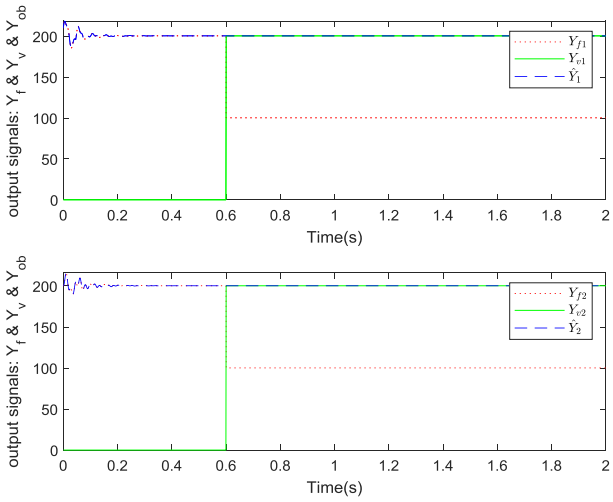

Fig. 10. The real outputs (red), estimated outputs (blue) and virtual sensor outputs (green)

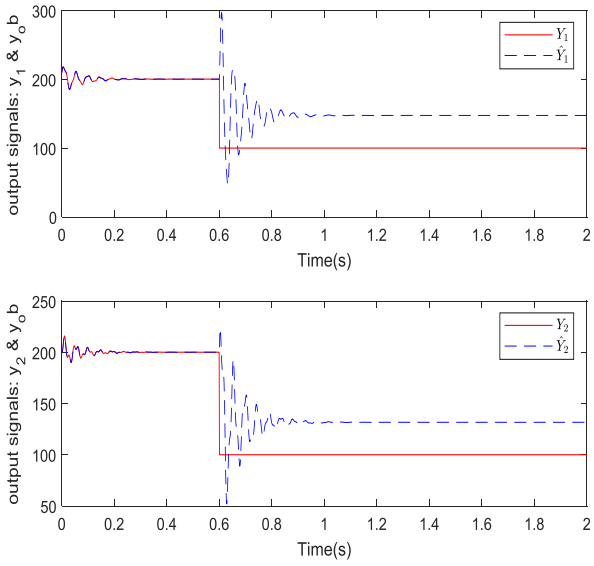

Fig. 11. The real outputs (red) and the estimated outputs (blue) in the absence of virtual sensor

In the absence of virtual sensor, the observer does not estimate the real outputs as it is depicted in Figure 11; but the designed virtual sensor when activated, hides the faults from the controller and the observer and as a consequence, the observer shows the same non-faulty output as before that it is seen in Figure 10. Comparing Figure 10 and Figure 11, reveals that the FTC strategy has operated properly with the virtual sensor The virtual sensor has done its task of completely hiding the fault from the observer and the controller perfectly.

In Figure 12, it can be seen that the observer states have converged to the nominal states of the plant. States 1 and 2 are related to current signals and states 3 and 4 are related to voltage signals. Also, the effect of the faults on the nominal plant and observer states can be analysed using the virtual sensor states. As shown in Figure.13, at the time of occurrence of the sensor faults, the virtual sensor is activated, thus prevents the faults from affecting the observer states.

For a better comparison, the effect of the faults on the observer when the virtual sensor is not activated is depicted in Figure 14. According to this figure, when the virtual sensor is not active, the faults directly affect the observer. The state estimation is not carried out correctly since the state estimates are deviated from the states' true values after the faults.

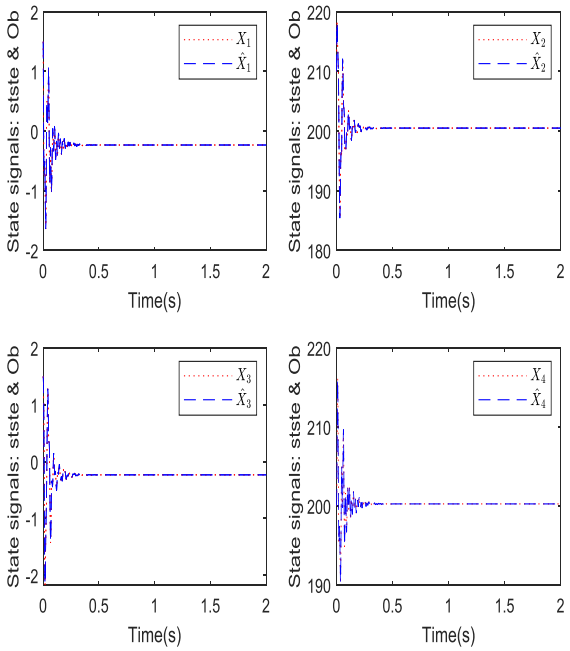

Fig. 12. System states and their estimates

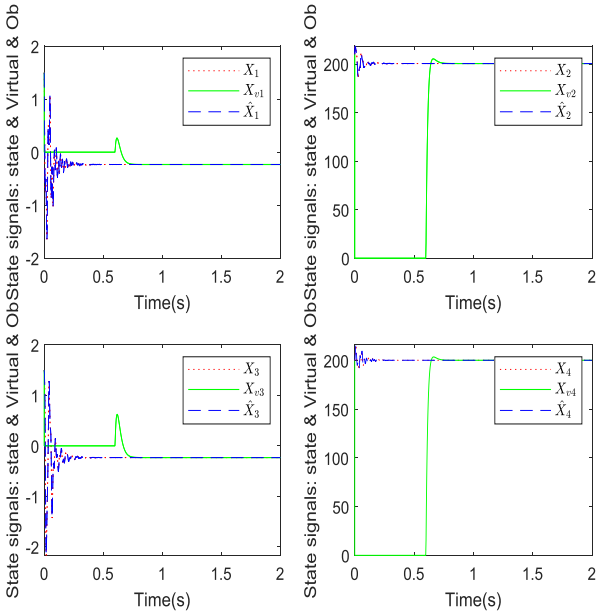

Fig. 13. States of the nominal plant (red), states of the observer (blue) and states of the virtual sensor (green)

One of the essential aspects of the current study is the analysis of the control signal that is applied to control the system in the presence of sensor fault in two modes of virtual sensor activation and virtual sensor inactivity despite the presence of the sensor fault. This allows us to observe the effect of the virtual sensor on the performance of the control signal. As it can be seen in Figure 15, despite the fault occurrence in 0.6 seconds, the virtual sensor causes the fault to be completely hidden from the observer, and due to the fact that the control signal is based on the observer output, the presence of fault has no effect on the control signal. In another simulation, the virtual sensor block is disactivated. So, in the event of a sensor fault, faulty outputs enter the observer as the inputs. As it is depicted in Figure 16, the control signal is fluctuated and settles down to another level after occurrence of the sensor fault in 0.6 seconds.

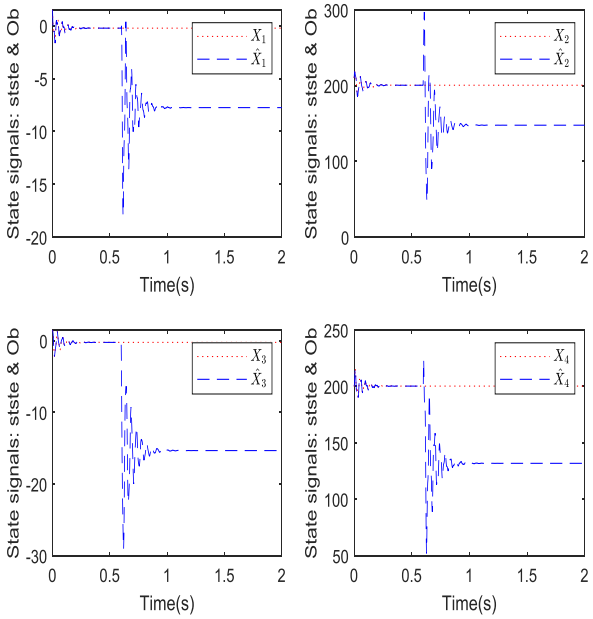

Fig. 14. Nominal system and observer states without virtual sensor activation

5. Conclusion

The purpose of this paper was to design an active fault-tolerant control strategy for sensor faults in a DC microgrid system. The nonlinear model of the considered microgrid consisting of constant power loads was presented, and then it was converted to a TS fuzzy model. The AFTC strategy was based on hiding the sensors' faults form the controller and the observer using a virtual sensor. Using appropriate LMI regions, the controller, the virtual sensor, and the observer were designed with suitable performance. The effectiveness of the proposed method was shown in the simulation.

Designing active fault-tolerant control for actuator faults hiding in this system using a suitable virtual actuator and the simultaneous design of the virtual sensor and virtual actuator to hide the effects of both sensors with actuator faults is part of the future lines of the current research.

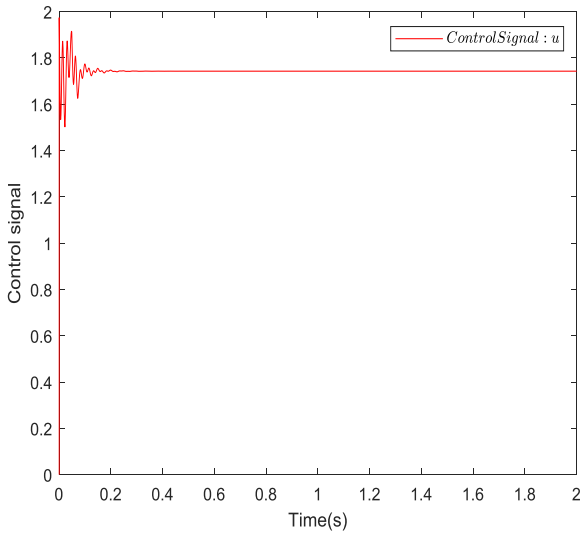

Fig. 15. Control signal in the presence of the virtual sensor

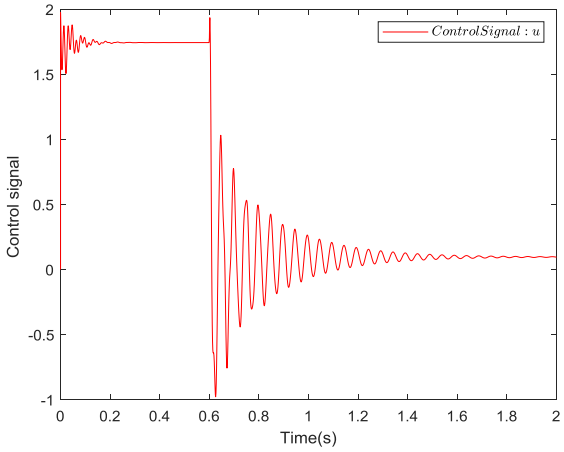

Fig. 16. Control signal in the absence of the virtual sensor

References

[1] S. Gholami, S. Saha, and M. Aldeen, "Fault tolerant control of electronically coupled distributed energy resources in microgrid systems," *International Journal of Electrical Power & Energy Systems*, vol. 95, pp. 327-340, 2018.

[2] L. Herrera, W. Zhang, and J. Wang, "Stability analysis and controller design of DC microgrids with constant power loads," *IEEE Transactions on Smart Grid*, vol. 8, no. 2, pp. 881-888, 2015.

[3] D. Marx, P. Magne, B. Nahid-Mobarakeh, S. Pierfederici, and B. Davat, "Large signal stability analysis tools in DC power systems with constant power loads and variable power loads—A review," *IEEE Transactions on Power Electronics*, vol. 27, no. 4, pp. 1773-1787, 2011.

[4] K. Rajesh, S. Dash, R. Rajagopal, and R. Sridhar, "A review on control of ac microgrid," *Renewable and sustainable energy reviews*, vol. 71, pp. 814-819, 2017.

[5] A. Bidram, V. Nasirian, A. Davoudi, and F. L. Lewis, "Control and modeling of microgrids," in *Cooperative synchronization in distributed microgrid control*: Springer, 2017, pp. 7-43.

[6] L. Sedghi, M. Emam, A. Fakharian, and M. Savaghebi, "Decentralized control of an islanded microgrid based on offline model reference adaptive control," *Journal of Renewable and Sustainable Energy*, vol. 10, no. 6, p. 065301, 2018.

[7] Q. Li, F. Chen, M. Chen, J. M. Guerrero, and D. Abbott, "Agent-based decentralized control method for islanded microgrids," *IEEE Transactions on Smart Grid*, vol. 7, no. 2, pp. 637-649, 2015.

[8] R. Nazari, M. M. Seron, and J. A. De Doná, "Fault-tolerant control of systems with convex polytopic linear parameter varying model uncertainty using virtual-sensor-based controller reconfiguration," *Annual reviews in control*, vol. 37, no. 1, pp. 146-153, 2013.

[9] S. M. Tabatabaeipour, J. Stoustrup, and T. Bak, "Control reconfiguration of LPV systems using virtual sensor and actuator," *IFAC Proceedings Volumes*, vol. 45, no. 20, pp. 818-823, 2012.

[10] J. Hare, X. Shi, S. Gupta, and A. Bazzi, "Fault diagnostics in smart micro-grids: A survey," *Renewable and Sustainable Energy Reviews*, vol. 60, pp. 1114-1124, 2016.

[11] D. Rotondo, F. Nejjari, and V. Puig, "A virtual actuator and sensor approach for fault tolerant control of LPV systems," *Journal of Process Control*, vol. 24, no. 3, pp. 203-222, 2014.

[12] J. Rodriguez-Guerra, C. Calleja, A. Pujana, I. Elorza, and A. M. Macarulla, "Fault-tolerant control study and classification: Case study of a hydraulic-press model simulated in real-time," *International Journal of Electrical and Information Engineering*, vol. 13, no. 2, pp. 115-127, 2019.

[13] Z. Gao, Z. Zhou, G. Jiang, M. Qian, and J. Lin, "Active fault tolerant control scheme for satellite attitude systems: Multiple actuator faults case," *International Journal of Control, Automation and Systems*, vol. 16, no. 4, pp. 1794-1804, 2018.

[14] Z. Gao, P. Cheng, M. Qian, G. Jiang, and J. Lin, "Active fault-tolerant control approach design for rigid spacecraft with multiple actuator faults," *Proceedings of the Institution of Mechanical Engineers, Part I: Journal of Systems and Control Engineering*, vol. 232, no. 10, pp. 1365-1378, 2018.

[15] M. J. Morshed and A. Fekih, "A fault-tolerant control paradigm for microgrid-connected wind energy systems," *IEEE Systems Journal*, vol. 12, no. 1, pp. 360-372, 2016.

[16] A. Vargas-Martínez, L. I. Minchala Avila, Y. Zhang, L. E. Garza-Castañón, and H. Badihi, "Hybrid adaptive fault-tolerant control algorithms for voltage and frequency regulation of an islanded microgrid," *international transactions on electrical energy systems*, vol. 25, no. 5, pp. 827-844, 2015.

[17] N. M. Dehkordi and V. Nekoukar, "Robust reliable fault tolerant control of islanded microgrids using augmented backstepping control," *IET Generation, Transmission & Distribution*, vol. 14, no. 3, pp. 432-440, 2019.

[18] S. Gholami, S. Saha, and M. Aldeen, "Sensor fault tolerant control of microgrid," in *2016 IEEE Power and Energy Society General Meeting (PESGM)*, 2016: IEEE, pp. 1-5.

[19] T. W. Long, E. L. Hanzevack, and W. L. Bynum, "Sensor fusion and failure detection using virtual

sensors," in *Proceedings of the 1999 American Control Conference (Cat. No. 99CH36251)*, 1999, vol. 4: IEEE, pp. 2417-2421.

[20] J. H. Richter, W. Heemels, N. van de Wouw, and J. Lunze, "Reconfigurable control of PWA systems with actuator and sensor faults: stability," in *2008 47th IEEE Conference on Decision and Control*, 2008: IEEE, pp. 1060-1065.

[21] S. M. de Oca, D. Rotondo, F. Nejjari, and V. Puig, "Fault estimation and virtual sensor FTC approach for LPV systems," in *2011 50th IEEE Conference on Decision and Control and European Control Conference*, 2011: IEEE, pp. 2251-2256.

[22] M. Luzar and M. Witczak, "Fault-tolerant control and diagnosis for LPV system with H-infinity virtual sensor," in *2016 3rd Conference on Control and Fault-Tolerant Systems (SysTol)*, 2016: IEEE, pp. 825-830.

[23] M. Oosterom and R. Babuska, "Virtual sensor for fault detection and isolation in flight control systems-fuzzy modeling approach," in *Proceedings of the 39th IEEE Conference on Decision and Control (Cat. No. 00CH37187)*, 2000, vol. 3: IEEE, pp. 2645-2650.

[24] A. H. Hassanabadi, M. Shafiee, and V. Puig, "Actuator fault diagnosis of singular delayed LPV systems with inexact measured parameters via PI unknown input observer," *IET Control Theory & Applications*, vol. 11, no. 12, pp. 1894-1903, 2017.

[25] A. H. Hassanabadi, M. Shafiee, and V. Puig, "Sensor fault diagnosis of singular delayed LPV systems with inexact parameters: an uncertain system approach," *International Journal of Systems Science*, vol. 49, no. 1, pp. 179-195, 2018.

[26] H.-B. Zeng, K. L. Teo, Y. He, and W. Wang, "Sampled-data-based dissipative control of TS fuzzy systems," *Applied Mathematical Modelling*, vol. 65, pp. 415-427, 2019.

[27] C. Lin, Q.-G. Wang, T. H. Lee, and B. Chen, "$ H_ {\infty} $ Filter Design for Nonlinear Systems With Time-Delay Through T–S Fuzzy Model Approach," *IEEE Transactions on Fuzzy Systems*, vol. 16, no. 3, pp. 739-746, 2008.

[28] S. K. Nguang, P. Shi, and S. Ding, "Fault detection for uncertain fuzzy systems: An LMI approach," *IEEE Transactions on Fuzzy Systems*, vol. 15, no. 6, pp. 1251-1262, 2007.

[29] L. Wu and D. W. Ho, "Fuzzy filter design for Itô stochastic systems with application to sensor fault detection," *IEEE Transactions on Fuzzy Systems*, vol. 17, no. 1, pp. 233-242, 2008.

[30] H. Dong, Z. Wang, J. Lam, and H. Gao, "Fuzzy-model-based robust fault detection with stochastic mixed time delays and successive packet dropouts," *IEEE Transactions on Systems, Man, and Cybernetics, Part B (Cybernetics)*, vol. 42, no. 2, pp. 365-376, 2011.

[31] H. Gao and T. Chen, "Stabilization of nonlinear systems under variable sampling: a fuzzy control approach," *IEEE Transactions on Fuzzy Systems*, vol. 15, no. 5, pp. 972-983, 2007.

[32] M. M. Mardani, N. Vafamand, M. H. Khooban, T. Dragičević, and F. Blaabjerg, "Design of quadratic D-stable fuzzy controller for DC microgrids with multiple CPLs," *IEEE Transactions on Industrial Electronics*, vol. 66, no. 6, pp. 4805-4812, 2018.

[33] S. M. de Oca and V. Puig, "Fault-tolerant control design using a virtual sensor for LPV systems," in *2010 Conference on Control and Fault-Tolerant Systems (SysTol)*, 2010: IEEE, pp. 88-93.

[34] N. Vafamand, M. H. Asemani, and A. Khayatian, "Robust ${L_1} $ Observer-Based Non-PDC Controller Design for Persistent Bounded Disturbed TS Fuzzy Systems," *IEEE Transactions on Fuzzy Systems*, vol. 26, no. 3, pp. 1401-1413, 2017.

[35] S. Yousefizadeh, J. D. Bendtsen, N. Vafamand, M. H. Khooban, T. Dragičević, and F. Blaabjerg, "EKF-based predictive stabilization of shipboard DC microgrids with uncertain time-varying load," *IEEE Journal of Emerging and Selected Topics in Power Electronics*, vol. 7, no. 2, pp. 901-909, 2018.

[36] D. Rotondo, V. Puig, and F. Nejjari, "A bank of virtual sensors for active fault tolerant control of LPV systems," in *2014 European Control Conference (ECC)*, 2014: IEEE, pp. 252-257.

[37] A. Radke and Z. Gao, "A survey of state and disturbance observers for practitioners," in *2006 American Control Conference*, 2006: IEEE, p. 6 pp.

[38] G.-R. Duan and H.-H. Yu, *LMIs in control systems: analysis, design and applications*. CRC press, 2013.

[39] J. F. Sturm, "Using SeDuMi 1.02, a MATLAB toolbox for optimization over symmetric cones," *Optimization methods and software*, vol. 11, no. 1-4, pp. 625-653, 1999.

[40] J. Lofberg, "YALMIP: A toolbox for modeling and optimization in MATLAB," in *2004 IEEE international conference on robotics and automation (IEEE Cat. No. 04CH37508)*, 2004: IEEE, pp. 284-289.